Rare Metal Materials and Engineering
Volume 48, Issue 3, March 2019
Available online at www.rmme.ac.cn

Science Press

Cite this article as: Rare Metal Materials and Engineering, 2019, 48(3): 0744-0750.

ARTICLE

Indentation Size Effect and Strain Hardening of Glassy $Cu_{29}Zr_{32}Ti_{15}Al_5Ni_{19}$ During Nanoindentation

Pi Jinhong[1,2], Yan Yanan[1], Wang Rongxiang[1], Wu Jili[3]

[1] Nanjing Institute of Technology, Nanjing 211167, China; [2] Jiangsu Key Laboratory of Advanced Structural Materials and Application Technology, Nanjing 211167, China; [3] Jiangsu University, Zhenjiang 212013, China

Abstract: High entropy bulk metallic glass (HE-BMG) $Cu_{29}Zr_{32}Ti_{15}Al_5Ni_{19}$ was investigated by a nanoindentation method in load-controlled, continuous stiffness measurement (CSM) and cyclic loading modes. The results show that pop-in event occurs in this alloy during nanoindentation. The applied load has a greater influence on the pop-in events than the loading rate. When the applied load is larger than 40 mN, obvious pop-in events can be observed in the loading curves even at high loading rates up to 5 mN/s. Indentation size effect exists in this alloy, as confirmed by a decrease in hardness with increasing the indentation load and a Meyer's index n less than 2. The fraction of energy dissipated during indentation (E_d) changes within the range of 54%~60%. Cyclic loading tests reveal an obvious hardening effect.

Key words: high entropy alloy; nanoindentation; indentation size effect; strain hardening

In the past decade, high entropy alloys (HEAs) and bulk metallic glasses (BMGs) have been investigated separately, although both they were viewed as complex metallic alloys [1]. In a conventional view, a HEA involves at least 5 components in equiatomic or near equiatomic ratio [2]. A recently developed definition of HEAs has simplified the component feature to 4[3] and extended the composition to non-equiatomic ratio at a range of 5 at%~35 at%. Thermodynamically, multiple components and high mixing entropy usually favor the stability of melt of the alloys and thus benefit the formation of non-crystalline phase during the solidification, especially rapid solidification[4]. Very recently, a series of BMGs with equimolar or near equimolar ratios, named as high-entropy bulk metallic glasses (HE-BMGs), have been successfully fabricated by rapid solidification method and show outstanding properties, such as high room temperature plasticity and very high strength [5-10]. This kind of new alloys provides an opportunity to study the similarity and difference between HEAs and BMGs.

Regarding the properties of HE-BMGs, Zhao et al[11,12] demonstrated that the Poisson's ratio of $Ti_{20}Zr_{20}Hf_{20}Be_{20}$-$(Cu/Ni)_{20}$ HE-BMG is above the critical value of 0.31~0.32, reaching 0.348, suggesting that this HE-BMG is intrinsically plastic. This finding agrees with the proposed ductile-brittle transition value of the Poisson's ratio in traditional BMGs. Nanoindentation has become a commonplace tool for the evaluation of mechanical properties at small scales and has the potential to provide the necessary answers to the fundamental deformation mechanism in amorphous materials, such as BMGs [13-17]. Hardness, by nanoindentation, is an important parameter for assessing the mechanical properties and deformation/failure mechanism. Generally, hardness (H) of a material should not depend strongly on the depth of indentation if the material is intrinsically hard. Interestingly, the indentation size effect (ISE), which is manifested as an increase in hardness with decreasing the indentation peak load (P_{max}), sometimes exists during the indentation [17-19]. In crystalline materials, the ISE is believed to be resulted from the generation and slipping of dislocations and the strain hardening[20,21]. Usually, ISE is not expected to occur in BMGs because of the absence of dislocations [17]. However,

Received date: March 14, 2018
Foundation item: National Natural Science Foundation of China (51601089); Innovation Training Program for College Students in Jiangsu Province (TB201702018)
Corresponding author: Pi Jinhong, Ph. D., Associate Professor, School of Materials Engineering, Nanjing Institute of Technology, Nanjing 211167, P. R. China, Tel: 0086-25-86118274, E-mail: pijinhong@njit.edu.cn

ISE of BMGs has actually been observed and investigated [17-19, 22]. Underlying ISE, there may be a conjectural mechanism for understanding the deformation/failure of (HE)-BMGs.

It is now well accepted that the formation of shear bands in BMGs is governed by so-called shear transformation zones (STZs) which act as nuclei for the shear bands and are responsible for collective shear deformations under the compressive stress[23,24]. In STZs, local diffusion-controlled rearrangements of the atomic positions and the free volume can lead to softening of the material and shear localization [23]. Pop-ins, the sudden displacement burst, can be observed in the loading part of the load-displacement curves of nanoindentation in the BMGs [25-27]. Pop-ins can reveal the incipient plasticity of materials [28]. On the other hand, pop-ins has been strongly correlated with the formation of the shear bands and thus may be closely associated with the plastic deformation and the ISE of BMGs and HE-BMGs.

In this paper, HE-BMG $Cu_{29}Zr_{32}Ti_{15}Al_5Ni_{19}$ was fabricated by suction casting in a water-cooled copper mold, and then was used to investigate the influence of indentation size and loading rate on mechanical behavior.

1 Experiment

A $Cu_{29}Zr_{32}Ti_{15}Al_5Ni_{19}$ (at%) alloy ingot was prepared by arc-melting high purity constituent elements (purity higher than 99.9 wt%) in a high-purity argon atmosphere and then cast into rods. The preparation of rod shape amorphous $Cu_{29}Zr_{32}Ti_{15}Al_5Ni_{19}$ was described in our previous work [29]. The rod shape sample (1 mm in diameter) was cut into small rods with a low speed diamond saw (SYJ 160, China). The ratio of height to radius of the rod samples was 2:1. All samples were mechanically polished to mirror finish before nanoindentation experiments were conducted at room temperature using Agilent G200 nanomechanical tester fitted with a Berkovitch diamond tip (TB21090). Load-controlled mode was used to investigate the effects of peak load (P_{max}) and loading rate on the nanoindentation response of the HE-BMG. The peak load changes from 10 mN to 200 mN at the loading rate of 1, 2, 3, 4 and 5 mN/s. A load holding period of 10 s was introduced at the peak load before unloading. When unloaded, 5% of the maximum load was maintained as a residual force, which is required to retain the contact with the indentation when examining the viscoelastic recovery of the indentation depth after unloading [30,31]. In the continuous stiffness measurement (CSM) mode, which was used to find the change in hardness and modulus with the penetration depth, the maximum depth limit of indentation was controlled to 1000 nm. Similarly, a 10 s holding was introduced at the peak load before unloading.

Cyclic loading mode, i.e. multiple loading and unloading, was used to investigate the reversibility of deformation and the strain hardening effect [31,32]. In this mode, the maximum load in the reloading segment is larger than the load in previous holding segment. 10% of the load in the previous holding segment was kept in each unloading segment to ensure the contact between the sample and the indenter tip. And the maximum applied loads of the last step were 60 and 100 mN. The loading rate was 5 mN/s. In each indentation mode, the unloading rate was kept the same as the loading rate. The thermal drift was controlled to be ±0.05 nm/s. The initial machine calibration was carried out on a fused silica standard specimen. At least 5 indentations were performed in each condition. The 3-dimentional topographies of typical residual indents were scanned by interactive indent scan program provided by Agilent G200 system.

2 Results and Discussion

2.1 Pop-ins

Fig.1 shows the typical load-displacement (*P*-*h*) curves (offset for clarity) of HE-BMG $Cu_{29}Zr_{32}Ti_{15}Al_5Ni_{19}$ at different loading from 10 mN to 200 mN. Clearly, at each loading rate and each applied load condition, the loading curves show great repeatability at the initial stage of loading. When the applied load exceeds 40 mN, pop-in events can be observed in the loading curves even at a high loading rate of up to 5 mN/s. With increasing the load, the more frequent the pop-ins occurs, the wider the burst displacement. On the other hand, when the load under 20 mN was applied, pop-ins can only be observed at the loading rates slower than 2 mN/s. For more clarity, the loading segments of the HE-BMG loaded to 10 mN and 200 mN at different loading rates are shown in Fig.2. It reveals that the pop-in behaviors are strongly affected by the loading rate. Alternatively, the load corresponding to the first pop-in shifts to higher value with increasing the loading rate. It has been extensively demonstrated that the pop-in behavior is the response to the multiplication and propagation of shear bands. The stress referring to the first pop-in indicates the minimum critical stress of the behavior of shear bands. For the loading rate effect, the small loading rates favor the fully performing of shear bands. On the other hand, the large loading rates easily increase the required stress of shear band behaviors due to the highly localized deformation under the indenter. It is also worth noticing that the burst displacement of first pop-in referring to the higher loading rates is larger than that referring to the smaller loading rates. Obviously, after a rapid loading, much energy is concentrated in a localized region under the indenter, and the unconstrained displacement of shear bands is also enlarged. In the previous work, massive investigations have indicated that the relatively higher strain rates generally deteriorate the plastic deformation of BMGs but usually enhance the failure stress. Unmistakably, the behaviors of shear bands of BMGs are similar under the compression.

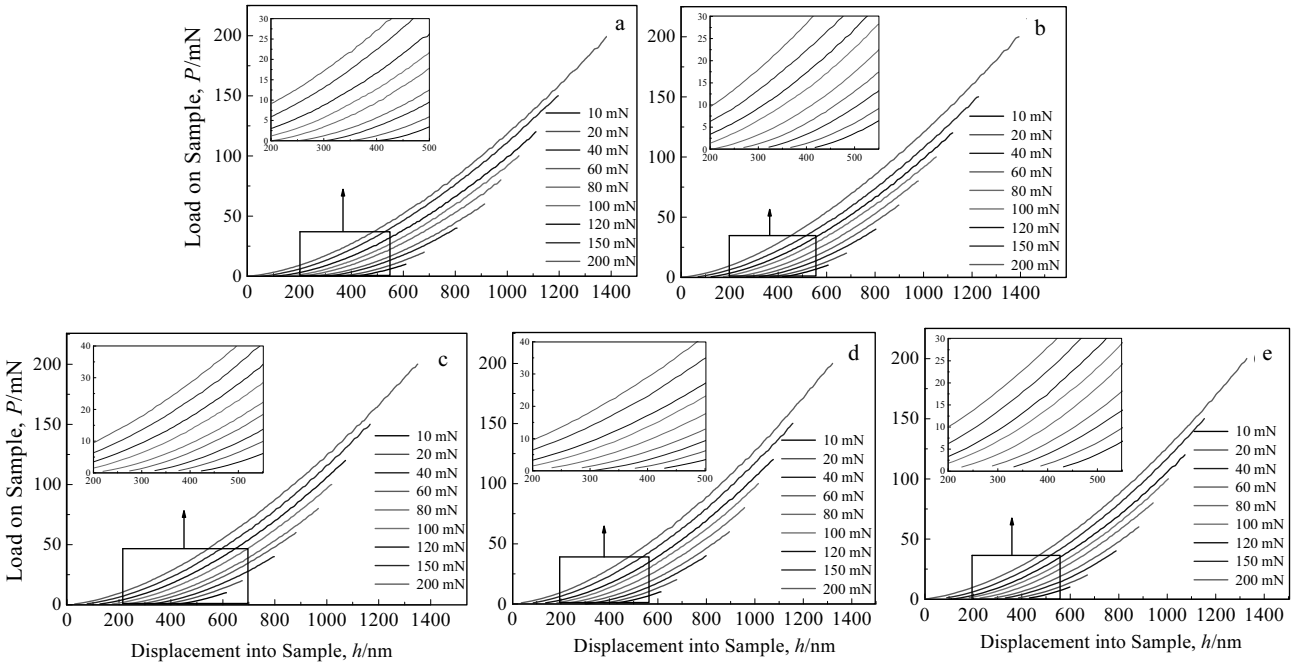

Fig.1 Typical load-displacement (*P-h*) curves of HE-BMG $Cu_{29}Zr_{32}Ti_{15}Al_5Ni_{19}$ at different loading rates: (a) 1 mN/s, (b) 2 mN/s, (c) 3 mN/s, (d) 4 mN/s, and (e) 5 mN/s

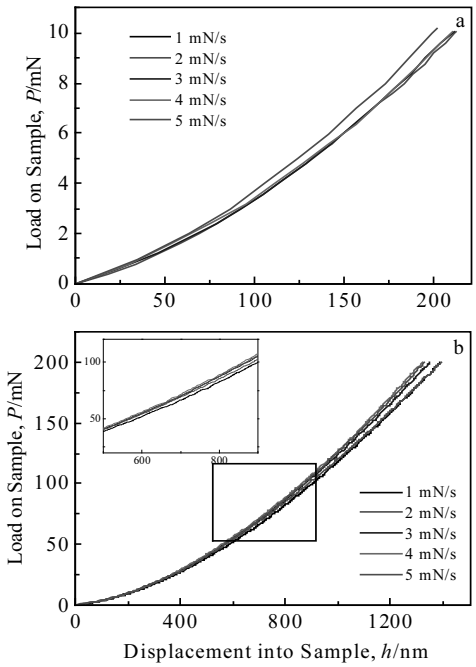

Fig.2 Typical loading segments of the load-displacement (*P-h*) curves of $Cu_{29}Zr_{32}Ti_{15}Al_5Ni_{19}$ at different applied loading rates with a maximum load of 10 mN (a) and 200 mN (b)

Fig.3 illustrates the typical residual indent morphology after indented at 5 mN/s. It clearly shows that there are no obvious cracks near the tip of the indentation. However, pile-ups at the edge of impressions can be clearly seen from Fig.3. Therefore, it is reasonable to suggest that the existence of pop-ins in this work is attributed to the formation and propagation of shear bands in the alloys rather than the cracks. Multiple pop-ins in the loading curves may be resulted from the interaction of shear bands near the tip of the indenter.

Frictions between the indenter and the surrounding materials may also slow the atomic migration beneath the indenter, which in turn leads to a decrease in the amount of pop-ins [31-33]. The slight variation in the locations of the pop-ins can be caused by the small perturbation of indentation conditions, such as a thermal drift, which is more influential to an indentation at a slower loading rate, and surface roughness can alter the local stress distribution in the neighborhood of the indentation zone [34]. When applied a larger load, more shear bands are triggered and propagated, resulting in more plastic deformation. And thus, more pop-ins can be observed.

2.2 Hardness, modulus and indentation size effect

According to Oliver and Pharr's theory, the hardness (*H*) in the nanoindentation can be calculated from the following equation [31,32].

$$H=P/A \quad (1)$$

where, *P* is the applied load and *A* is the contact area during indentation. For a Berkovich indenter, the projected area (*A*) can be fitted by:

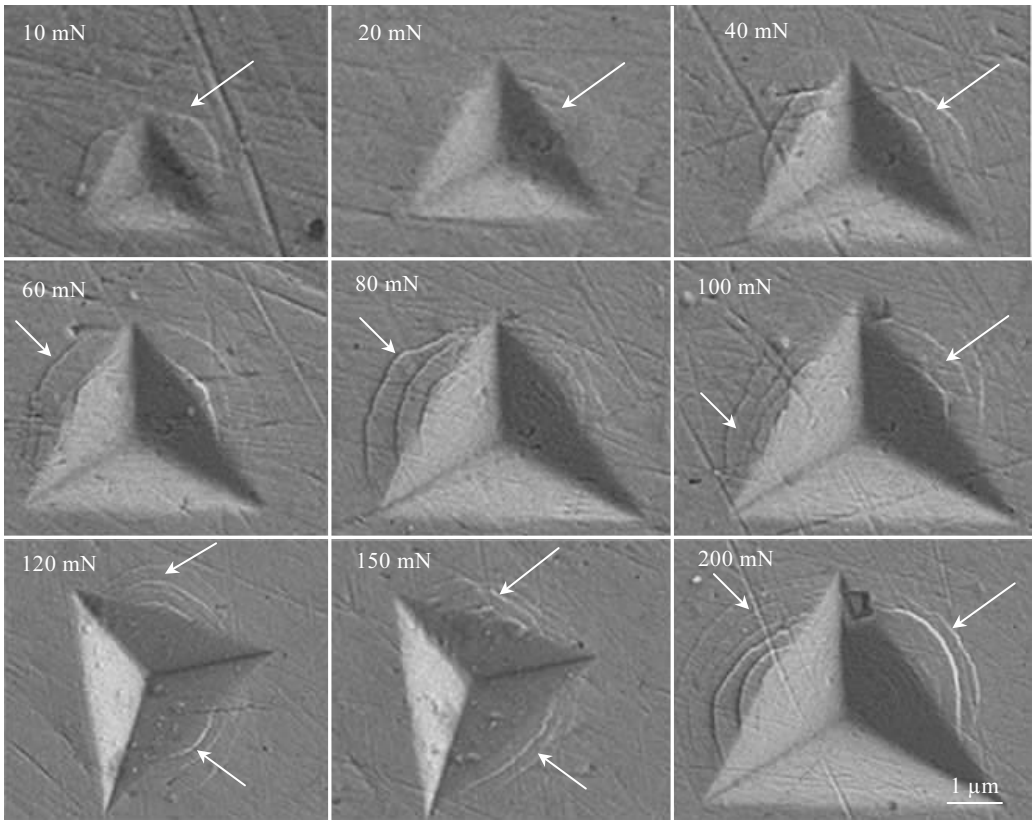

Fig.3 Typical residual indent morphologies of $Cu_{29}Zr_{32}Ti_{15}Al_5Ni_{19}$ at a loading rate of 5 mN/s

$$A=\sum_{n=0}^{8}c_n(h_c)^{\left(\frac{1}{2^{(n-1)}}\right)}=c_0h_c^{\ 2}+c_1h_c+c_2h_c^{\frac{1}{2}}+c_3h_c^{\frac{1}{4}}+\cdots+c_n(h_c)^{\left(\frac{1}{2^{(n-1)}}\right)}+c_8h_c^{\frac{1}{128}} \quad (2)$$

where, h_c is the depth of the residual impressions. For sink-ins occurred samples, the relationship between h_c and h_{max} is schematically shown in Fig.4. h_r is the intercept of the tangent to the initial unloading curve, h_{max} is the maximum penetration beneath the specimen surface, and P_{max} is the maximum load applied to the indenter. The area function calibration of the indenter tip was measured prior to the indentation.

The reduced modulus can be calculated as follows.

$$E_r=\frac{1}{2}\frac{\sqrt{\pi}}{\sqrt{A}}\frac{dP}{dh} \quad (3)$$

$$\frac{1}{E_r}=\frac{(1-\nu^2)}{E}+\frac{(1-\nu_i^2)}{E_i} \quad (4)$$

where E_r is the reduced modulus, ν is the Poisson's ratio for the specimen, and E_i and v_i are the parameters of the indenter.

If the indentation size effect (ISE) exists in HE-BMG $Cu_{29}Zr_{32}Ti_{15}Al_5Ni_{19}$, the tested hardness which decreases with increasing the indentation load or indentation depth will be

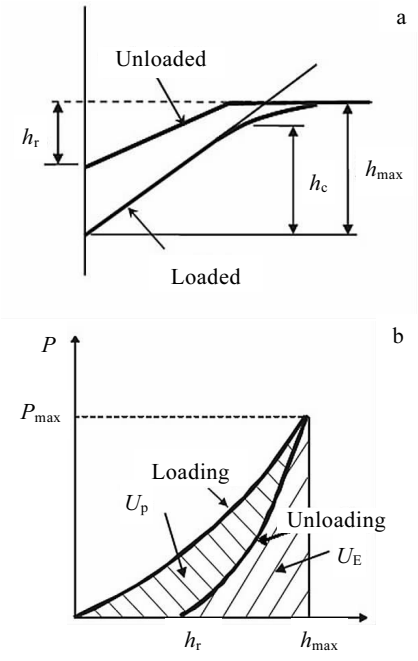

Fig.4 Schematic of indentation test procedure

observed. Fig.5 shows the typical curves of hardness and modulus of $Cu_{29}Zr_{32}Ti_{15}Al_5Ni_{19}$. Fig.6 shows the calculated values of hardness and modulus under different maximum loads and loading rates.

From Fig.5, after an initial sharp increase, the values of hardness and modulus do decrease as the indentation depth increases and tend to stabilize at the deep penetration. The experimental results confirmed that strong ISE exists in HE-BMG $Cu_{29}Zr_{32}Ti_{15}Al_5Ni_{19}$ during the nanoindentation within the range of 100 nm. As illustrated in Fig.3, obvious pile-ups (pointed by arrows) formed in the tested samples during penetration. And more pile-ups formed as the penetration depth increased, resulting in an increase in the density of shear bands. In other words, more diffusion-controlled STZs formed. Meanwhile, the strain gradients in the vicinity of the indentation formed. As a result, the rearrangements of atomic positions and free volume lead to a softening. While in HE-BMGs, the rearrangements of atoms are sluggish due to the high entropy effect and the strong metallic bonds among the multiple elements. That is why ISE exists in the tested HE-BMG samples although the ISE is more pronounced in soft materials.

The slight oscillating of hardness and modulus at the stable stage may be resulted from the pop-in events mentioned above.

From Fig.6, both hardness and modulus at the peak load decrease with the applied load. And the effect of maximum applied load on the values of modulus is greater than that on the hardness. Loading rates have less influence on the modulus and hardness than maximum applied load.

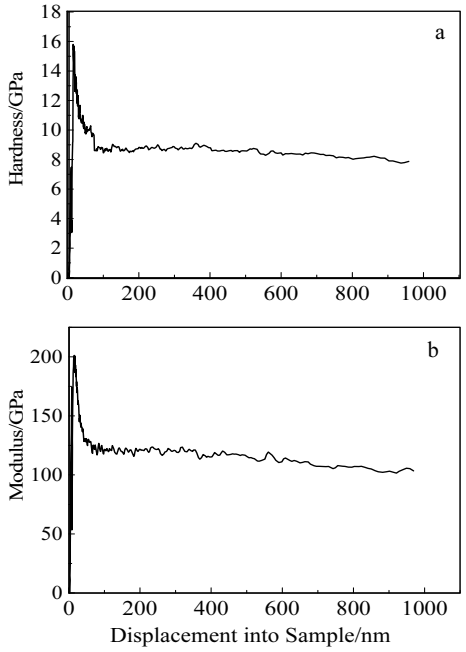

Fig.5 Typical hardness-displacement (a) and modulus-displacement (b) curves of $Cu_{29}Zr_{32}Ti_{15}Al_5Ni_{19}$ by CSM mode

According to Meyer's law, if the indenter has an ideal geometry, the relationship between the applied load (P) and the indentation depth (h) can be expressed as follows [33]:

$$P=C h^n \tag{5}$$

where C is a constant. And the second-order differential against indentation depth h in Eq.(5) can be provided by:

$$\frac{\mathrm{d}^2P}{\mathrm{d}^2h}=n(n-1)Ch^{n-2} \tag{6}$$

If n=2 in Eq. (5) and Eq.(6), the materials showed no ISE. If n<2, the materials showed ISE, which was confirmed by many materials [33]. The calculated values of n during loading to different P_{max} at a loading rate from 1 mN/s to 5 mN/s are shown in Fig.7.

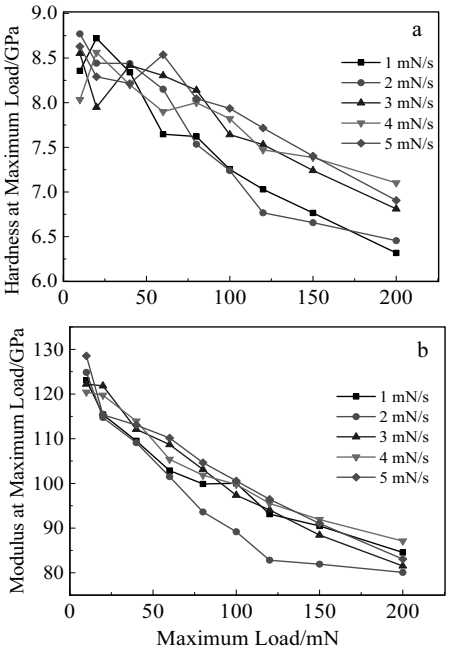

Fig.6 Hardness (a) and modulus (b) at different maximum applied loads

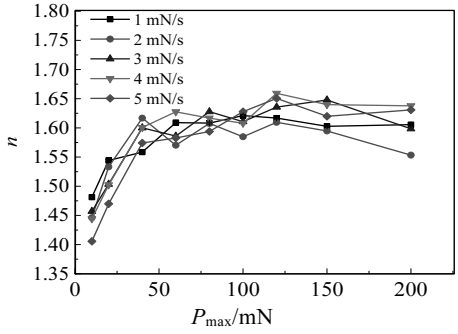

Fig.7 Index n vs P_{max} at different loading rates

From Fig.7, the values of index n at all testing conditions are less than 2, indicating the existence of ISE during the indention of glassy $Cu_{29}Zr_{32}Ti_{15}Al_5Ni_{19}$. And n increases with the P_{max} when P_{max} < 60 mN. After that, the values of n show a very slight change.

Generally speaking, a significant indentation size effect is expected for soft materials, but very small indentation size effect is expected for hard materials [31]. It is interesting that the HE-BMG shows both obvious ISE and high hardness (see Fig.6).

2.3 Energy dissipation

The fraction of energy dissipated during indentation, E_d, is determined by calculating the area within the indentation p-h curve divided by the area under the loading portion of the curve [35]. In other words, E_d can be simply calculated by the following equation:

$$E_d = \frac{U_p}{U_p + U_e} \quad (7)$$

where U_p is the net area enclosed by the load-displacement curve (see Fig.4b), representing the energy loss due to plastic deformation and elastic strains for residual stresses in the specimen material, and U_e represents the area beneath the unloading curve. Pure plastic work is dissipated as heat (E_d=100%). Pure elastic deformation does not dissipate energy and is fully recovered upon unloading (E_d=0%). The calculated energy dissipation fraction E_d of HE-BMG $Cu_{29}Zr_{32}Ti_{15}Al_5Ni_{19}$ loaded to different P_{max} is shown in Fig.8. It can be clearly seen that all calculated values of E_d change within the range of 54%~60%.

2.4 Strain hardening effect

The typical load-displacement curves under cyclic loading are shown in Fig.9. From Fig.9, obvious hysteresis in the reloading curves can be observed. In other words, the unloading curve is not completely reversible for the subsequent reloading curve. Higher load is needed to reach the same indentation depth as the previous unloading. During cyclic nanoindentation, the sample is loaded and unloaded

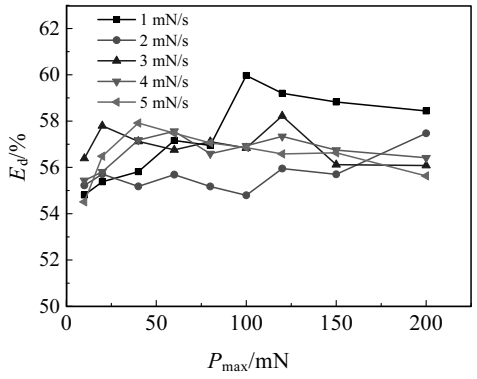

Fig.8 Energy dissipation fraction E_d vs P_{max} of glassy $Cu_{29}Zr_{32}Ti_{15}Al_5Ni_{19}$

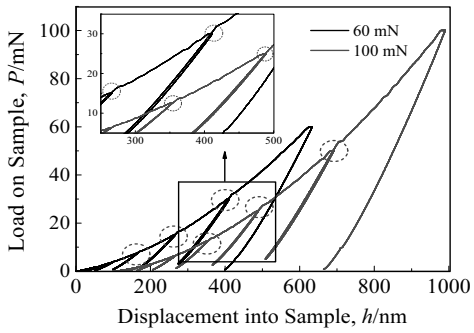

Fig.9 Typical load-displacement curves undercyclic loading

repeatedly at the same position, resulting in the formation of hysteresis loop, which is a direct evidence of the reverse plasticity of the material during unloading. In the reloading curve, the slope of the load-displacement curve changes after a yielding point as marked by the circle in Fig.9, which exhibits a hardening effect [30]. And the higher the applied load, the stronger the strain hardening effect.

Unlike the conventional loading mode, cyclic loading can boost the events of pop-ins. Even when the applied load is less than 20 mN, clear serration flows can be observed at a loading rate up to 5 mN/s. Larger load or slower loading rate is needed to trigger the pop-ins in the usual one time loading-unloading mode (see Fig.1 discussed above).

3 Conclusions

1) Pop-in occurs in HE-BMG $Cu_{29}Zr_{32}Ti_{15}Al_5Ni_{19}$ during nanoindentation.

2) Applied load has more influences on the pop-in events than loading rate.

3) Indentation size effect exists in HE-BMG $Cu_{29}Zr_{32}Ti_{15}Al_5Ni_{19}$, as confirmed by the decreasing hardness with increasing the indentation load and the Meyer's index n less than 2. The fraction of energy dissipated during indentation (E_d) changes within the range of 54%~60%.

References

1 Gong P, Yao K F, Ding H Y. *Materials Letters*[J], 2015, 156: 146

2 Zhao S F, Yang G N, Ding H Y *et al. Intermetallics*[J], 2015, 61: 47

3 Qi Tianlong, Li Yanhui, Takeuchi A *et al*. *Intermetallics*[J], 2015, 66: 8

4 Suryanarayana C, Inoue A. *Bulk metallic glasses*[M]. New York: CRC Press, 2011

5 Chen C, Pang S J, Cheng Y Y *et al*. *Journal of Non-Crystalline Solids* [J], 2015, 410: 39

6 Takeuchi A, Chen N, Wada T *et al*. *Intermetallics*[J], 2011, 19: 1546

7 Tripathi M K, Chattopadhyay P P, Ganguly S. *Computational* Materials *Science*[J], 2015, 107: 79
8 Satish Idury K S N, Murty B S, Bhatt J. *Intermetallics*[J], 2015, 65: 42
9 Takeuchi A, Chen N, Wada T *et al*. *Procedia Engineering*[J], 2012, 36: 226
10 Gao X Q, Zhao K, Ke H B *et al*. *Journal of Non-Crystalline Solids* [J], 2011, 357: 3557
11 Zhao S F, Yang G N, Ding H Y *et al*. *Intermetallics*[J], 2015, 61: 47
12 Zhao S F, Shao Y, Liu X *et al*. *Materials and Design*[J], 2015, 87: 625
13 Wu J L, Pan Y, Pi J H. *Journal of Materials Engineering and Performance*[J], 2013, 22: 2288
14 Zhu L N, Xu B S, Wang H D *et al*. *Critical Reviews in Solid State and Materials Sciences*[J], 2015, 40(2): 77
15 Mukhopadhyay N K, Paufler P. *International Materials Reviews*[J], 2006, 51(4): 209
16 Schuh C A. *Materials Today*[J], 2006, 9(5): 32
17 Schuh C A, Nieh T G. *Journal of Materials Research*[J], 2004, 19(1): 46
18 Xu F, Ding Y H, Deng X H *et al*. *Physica B*[J], 2014, 450: 84
19 Mukhopadhyay N K, Belger A, Paufler P *et al*. *Materials Science and Engineering A*[J], 2007, 449-451: 954
20 Chatterjee A, Srivastava M, Sharma G *et al*. *Materials Letters*[J], 2014, 130: 29
21 Wang M, Wang D, Kups T *et al*. *Materials Science and Engineering A*[J], 2015, 644: 275
22 Li N, Liu L, Chan K C *et al*. *Intermetallics*[J], 2009, 17: 227
23 Haag F, Beitelschmidt D, Eckert J *et al*. *Acta Materialia*[J], 2014, 70: 188
24 Bhattacharyya A, Singh G, Prasad K E *et al*. *Materials Science and Engineering A*[J], 2015, 625: 245
25 Cao Q P, Jin J B, Ma Y *et al*. *Journal of Non-Crystalline Solids*[J], 2015, 412: 35
26 Wu J L, Pan Y, Pi J H. *Journal of Materials Engineering and Performance*[J], 2014, 23: 486
27 Medeiros B B, Medeiros M M, Fornell J *et al*. *Journal of Non-Crystalline Solids*[J], 2015, 425: 103
28 Caër C, Patoor E, Berbenni S *et al*. *Materials Science and Engineering A*[J], 2013, 587: 304
29 Pi J H, Wang Z Z, He X C *et al*. *Journal of Materials Engineering and Performance*[J], 2016, 25: 76
30 Wang Z J, Guo S, Wang Q *et al*. *Intermetallics*[J], 2014, 53: 183
31 Fischer-Cripps A. *Nanoindentation, Third Ed*[M]. New York: Springer, 2011
32 Li X D, Bhushan B. *Materials Characterization*[J], 2002, 48: 11
33 Ebisu T, Horibe S. *Journal of the European* Ceramic *Society*[J], 2010, 30: 2419
34 Chang L, Zhang L C. *Materials Science and Engineering A*[J], 2009, 506: 125
35 Dar R D, Chen Y. *Acta Materialia*[J], 2015, 91: 112

玻璃态 $Cu_{29}Zr_{32}Ti_{15}Al_5Ni_{19}$ 在纳米压入过程中的压痕尺寸效应及应变硬化现象

皮锦红[1,2], 严亚楠[1], 汪荣香[1], 吴继礼[3]

(1. 南京工程学院，江苏 南京 211167)

(2. 江苏省先进结构材料与应用技术重点实验室，江苏 南京 211167)

(3. 江苏大学，江苏 镇江 212013)

摘　要：利用纳米压痕技术对高熵非晶合金 $Cu_{29}Zr_{32}Ti_{15}Al_5Ni_{19}$ 分别在载荷控制模式、连续刚度模式和循环加载模式下进行了研究。该合金在纳米压入过程中会发生 pop-in 现象，且载荷大小比加载速率对 pop-in 现象的影响更大。当载荷超过 40 mN 时，即使采用高达 5 mN/s 的加载速率仍然可以观察到 pop-in 现象。该合金存在压痕尺寸效应，其测试纳米硬度随载荷的增大而下降，其 Meyer 指数(n)小于 2。压入过程中的能量耗散分数(E_d)在 54%~60%之间变化。循环加载测试结果显示该合金加工硬化效应明显。

关键词：高熵合金；纳米压痕；压痕尺寸效应；加工硬化

作者简介：皮锦红，女，1977 年生，博士，副教授，南京工程学院材料工程学院，江苏 南京 211167，电话：025-86118274，E-mail: pijinhong@njit.edu.cn